

Contents lists available at [SciVerse ScienceDirect](http://www.sciencedirect.com)

Physics of the Earth and Planetary Interiors

journal homepage: www.elsevier.com/locate/pepi

On the detectability of 3-D postperovskite distribution in D'' by electromagnetic induction

Jakub Velínský*, Nina Benešová, Hana Čížková

Department of Geophysics, Faculty of Mathematics and Physics, Charles University in Prague, Czech Republic

ARTICLE INFO

Article history:

Received 22 June 2011

Received in revised form 23 November 2011

Accepted 22 February 2012

Available online xxx

Edited by Kei Hirose

Keywords:

D''

Geomagnetic induction

Electrical conductivity

ABSTRACT

1-D global inversions of observatory and satellite geomagnetic data reveal radial conductivity profiles in the Earth's mantle by means of electromagnetic induction. Traditionally, these have been interpreted as average values at given depth. However, the predominant dipolar geometry of the magnetospheric ring current represents strong bias in 1-D interpretation of the responses of a fully 3-D heterogeneous Earth. We present a series of synthetic checks, applying 1-D time-domain inversion technique to 3-D simulated data for conductivity models with lateral heterogeneities in the lowermost mantle, ranging from simple geometrical configurations to complicated structures derived from phase composition based on geodynamical modelling. We show that it is the presence or lack of lateral interconnection of the highly conductive phase in the direction of prevailing external currents that determines the results of 1-D inversion. In particular, this effect can explain the recently shown invisibility of highly conductive postperovskite in the D'' layer to induction studies excited by strong transient signals—the geomagnetic storms.

© 2012 Elsevier B.V. All rights reserved.

1. Introduction

In contrast to the upper mantle where our understanding of the structure and processes has improved considerably in the last decades, the lower mantle still remains much less explored. Perhaps the most enigmatic part of the lower mantle is its lowermost part, the D'' . The investigations focused on this area received a new impetus in 2004, when a high pressure mineral phase, the postperovskite (PPV), has been discovered (Murakami et al., 2004; Oganov and Ono, 2004; Tsuchiya et al., 2004). Since then numerous studies addressed the issues related to PPV morphology (e.g., Hernlund et al., 2005; van der Hilst et al., 2007; Shim, 2008; van den Berg et al., 2010), seismic anisotropy (Panning and Romanowicz, 2006; Wookey and Kendall, 2008), transport properties (Oganov and Ono, 2005; Carrez et al., 2007; Walte et al., 2007; Hunt et al., 2009; Ammann et al., 2010; Goncharov et al., 2010; Ono et al., 2006; Ohta et al., 2008, 2010), and dynamic consequences (Nakagawa and Tackley, 2004, 2005, 2006; Matyska and Yuen, 2005; Monnerneau and Yuen, 2007; Tackley et al., 2007; Čížková et al., 2010; Tosi et al., 2010).

A large Clapeyron slope of the PPV exothermic phase transition—13 MPa/K (Tateno et al., 2009)—together with a steep temperature gradient in the bottom thermal boundary layer probably result in the double-crossing of the phase boundary and thus the isolated lenses of PPV are expected to exist in the lower mantle

(Hernlund et al., 2005) in the relatively cold areas. Seismic observations indeed support the existence of isolated patches of PPV in the lowermost mantle (e.g., Lay et al., 2006; van der Hilst et al., 2007; Hutko et al., 2008). A possible source of information about the spatial distribution of PPV lenses in the lower mantle could be the observed seismic anisotropy. It has been shown that the dislocation creep localization in the PV in lowermost mantle beneath the slabs could produce the observed lattice preferred orientation, but it is not able to explain the amplitude of the observed anisotropy. For this the PPV could be responsible (Oganov and Ono, 2005; Shim, 2008). The distribution of the lowermost mantle seismic anisotropy as reported by Panning and Romanowicz (2006) shows the predominance of the horizontally polarized S-wave velocity over the vertically polarized one in the circum-Pacific belt, which supports the idea, that the PPV should be present only in the relatively cold areas connected to paleoslabs.

Despite the growing seismic evidence, an independent information constraining the PPV positions would be extremely useful. Based on several experimental as well as theoretical works, PPV is now expected to differ from perovskite (PV) in terms of transport properties. Its viscosity is expected to be considerably weaker (e.g., Hunt et al., 2009; Ammann et al., 2010), while the electrical conductivity of PPV has been reported to be by up to 2 orders of magnitude higher than that of PV (Ono et al., 2006; Ohta et al., 2008, 2010). The conductivity anomaly of this order (though buried in the deepest mantle) should be reflected in the geomagnetic data. The electromagnetic (EM) induction by variations of external fields requires long-periodic or strong transient excitation in order to de-

* Corresponding author.

E-mail address: jakub.velinsky@mff.cuni.cz (J. Velínský).

tect deep mantle structures. Geomagnetic storms, excited by the Sun, and manifested in the magnetosphere by energizing of the equatorial ring current, represent such a signal. It is capable of inducing secondary electric currents in the deepest regions of the Earth, including the core (Velínský and Finlay, 2011). The magnetic field generated by the ring current has dominantly dipolar structure in the geomagnetic coordinate system defined by the Earth's main field, although smaller non-axisymmetric contributions are also present (Balasis et al., 2004). While numerical methods for global 3-D inversion of geomagnetic data are available and computationally feasible, so far they have been applied only to the upper parts of the mantle (Kelbert et al., 2009), down to the depth of 1600 km. Below that, available data allow only to study the 1-D conductivity. A 1-D conductivity profile obtained by Velínský (2010) in the inversion of CHAMP satellite data did not show any significant increase in D'' and thus did not agree with the experimental data by Ono et al. (2006) and Ohta et al. (2008, 2010). However, that does not necessarily mean, that a highly conductive PPV is not present there. If the PPV does not form a continuous layer, but rather isolated patches, their high conductivity may not show up unless they are interconnected in the equatorial direction, that is in the direction of prevailing external currents. Here we test this possibility by performing a synthetic EM inversion. We suggest several models of the 3-D distribution of the highly conductive PPV in the lowermost mantle, calculate their induction response and then perform an inversion looking for the 1-D depth dependent conductivity profile. We demonstrate that the geometry of a highly conductive PPV patches is crucial for their visibility in terms of 1-D conductivity distribution.

The paper is organized as follows: In Section 2 we define six synthetic conductivity models with different D'' structure. In Section 3 we compute the 3-D induction response of these models to quasi-realistic magnetospheric excitation. We follow up by 1-D inversion of synthetic data in Section 4, discuss the statistical significance of our results in Section 5, and conclude with Section 6.

2. Synthetic conductivity models

The amplitude of lateral conductivity variations in the Earth varies with depth. Closest to the surface, the contrast between

highly conductive seawater, conductive sediments, and resistive igneous rocks yields lateral variations of more than 3 orders of magnitude when scaled to a common thickness (Everett et al., 2003). In the upper mantle, especially in the transition zone, the conductivity varies by more than one order due to the variations in temperature, partial melt distribution, and water content (Kelbert et al., 2009). Recently, Tarits and Manda (2010) have obtained significant variations also in the lower mantle by inversion of geomagnetic observatory monthly means.

In this study, we are interested in the effect of the complex D'' structure on the EM induction data, and on the ability of the EM inversion to resolve such a structure. Therefore, our models assume a 3-D laterally variable conductivity just above the core-mantle boundary, while in the rest of the lower mantle a 1-D depth dependent conductivity is considered. Such simplified models could be regarded as best case scenarios, in reality the effects of the complex D'' conductivity are further shielded and obscured by the more complicated structures above.

The background 1-D conductivity model (Fig. 1, right panel) is based on the inversion of 7-years of geomagnetic data provided by the CHAMP satellite (Velínský, 2010). Here we use a model obtained for mixed parametrization with 100 km resolution in the upper mantle, and 400 km resolution in the lower mantle. The model also contains a core with conductivity of 10^5 S/m, also constrained by the CHAMP data, at least at the lower limit. The total number of layers is $K = 16$.

We introduce six different conductivity structures A–F (cf. Fig. 1, spherical inserts) which overlay the background 1-D model in the lowermost mantle. Models A and B are extreme cases, assuming homogeneous, 300 km thick D'' consisting of pure PV and PPV, respectively. The electrical conductivities assigned to the two phases are $\sigma_{PV} = 7$ S/m, and $\sigma_{PPV} = 100$ S/m (Ohta et al., 2008). The dependence on temperature is also neglected.

In models C and D, the 300 km thick D'' consists of PV with 1600 km wide circular belt of PPV placed along the equator, and along the $\pm 90^\circ$ meridian, respectively. The content of PPV in both models is the same (33% of the D'' volume). Therefore, we can study the effect of relative orientation of the closed loop of highly conductive PPV with respect to the dominantly dipolar geometry of the external field.

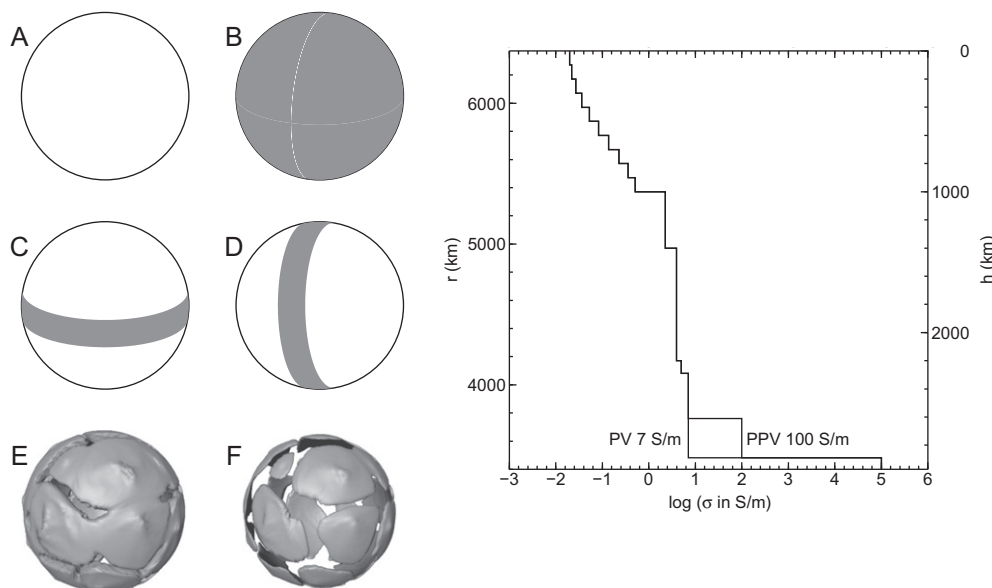


Fig. 1. Overview of synthetic electrical conductivity models used in this study. Right panel: background 1-D conductivity profile. Spherical inserts A–D: PPV structure (gray) in D'' with assumed thickness of 300 km in respective models. Spherical inserts E and F: Isosurfaces of the phase function $\phi(\mathbf{r}) = 0.5$ in respective models.

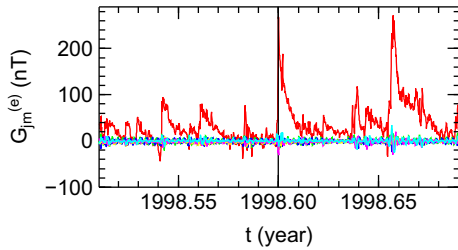


Fig. 2. Synthetic model of the external field. Here we show only a short excerpt spanning two months. Dipolar term which is shown in red is dominant over higher harmonics (here shown only up to degree 2 by various colors). The black vertical line at 1998.5995 marks the position of the snapshot of electrical currents in Fig. 3.

Finally, in models E and F, electrical conductivity distribution in the lowermost 600 km of the mantle is given by relation,

$$\log \sigma(\mathbf{r}) = (1 - \phi(\mathbf{r})) \log \sigma_{\text{PV}} + \phi(\mathbf{r}) \log \sigma_{\text{PPV}}. \quad (1)$$

Here $\phi(\mathbf{r})$ ranging from 0 to 1 is the phase function representing the volume fraction of PPV. It is based on the temperature distribution obtained in the 3-D spherical model of mantle convection. Model case E has an intercept temperature of 3900 K that produces an almost continuous layer of PPV interrupted only in the hot plume regions. In case F a very low temperature intercept of 3000 K ensures the existence of fully isolated conductive patches of PPV.

3. 3-D forward modelling

Each of the target conductivity models A–F, introduced in the previous section, is excited by a synthetic model of the external

field, similar to the one used in the end-to-end preparatory simulations for the Swarm satellite mission (Tøffner-Clausen et al., 2010). The model has been derived from the hourly means of magnetic field measured at permanent geomagnetic observatories. It describes quasi-realistic magnetospheric field variations by spherical harmonics up to degree 3 and order 1, and spans the period of 12 years with 1 h sampling rate, starting on January 1, 1997. Should we aim to invert realistic observatory or satellite data in terms of mantle conductivity, a careful consideration of the source model geometry would be needed (Fujii and Schultz, 2002; Kelbert et al., 2009; Martinec and Velínský, 2009). Since our goal is to study the effects of laterally heterogeneous D'' using artificial conductivity distributions, the synthetic external field model is sufficient for our purposes. Fig. 2 shows the spherical harmonic coefficients of the external field, $G_{jm}^{(e)}$, up to degree 2 during a two-month interval cut out from the entire span of the model. Two large geomagnetic storms occurred during this period. Note that following Velínský and Martinec (2005) we use orthonormal, complex spherical harmonics, and the coefficients are rescaled from the Schmidt semi-normalization accordingly. The model features a large dipolar term and much smaller variations at higher spherical harmonics, dominated by the diurnal period.

We use the time-domain 3-D forward solver of Velínský and Martinec (2005) which is based on mixed spherical harmonic-finite element spatial discretization, to compute the magnetic field \mathbf{B} in the entire conductive Earth. The time integration uses 1 h time step, the radial discretization uses 180 layers with 20 km resolution throughout the mantle, and 100 km resolution in the core. The lateral resolution is given by truncation degree of spherical harmonics, $j_{\text{max}} = 16$.

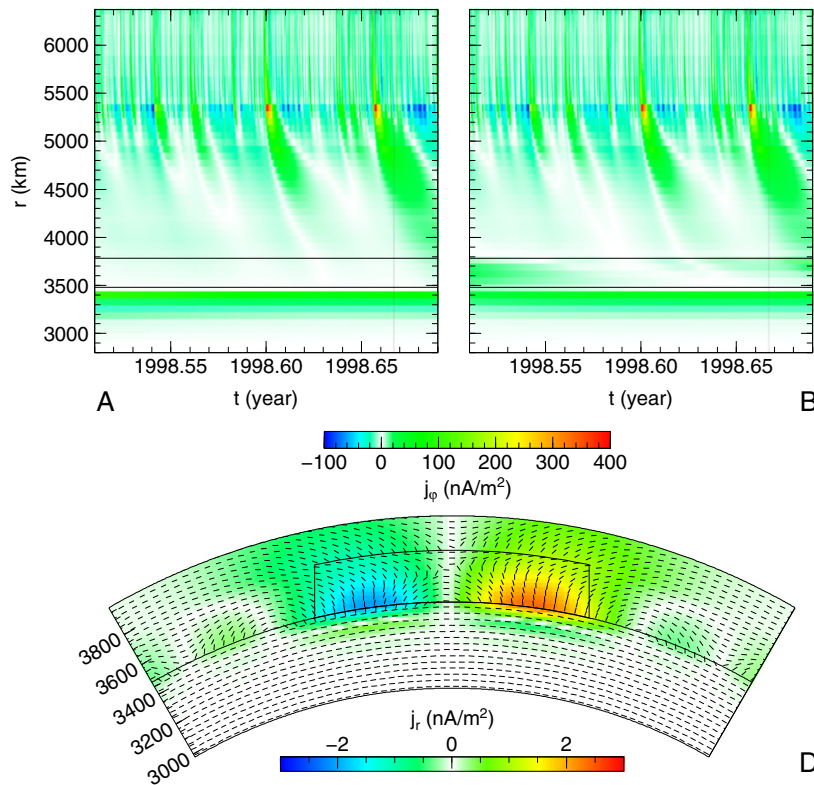


Fig. 3. Electrical currents induced in the Earth for conductivity models A, B, and D. We show the longitudinal component of current density j_ϕ at equator as a function of radius r and time t in case of spherically symmetric models A and B (top left and right, respectively). The CMB, and the D'' upper boundary are emphasized by solid black lines. A snapshot at $t=1998.5995$ years in an equatorial section in the vicinity of CMB, through the meridional high-conductivity band (marked by solid black lines) is plotted for model D (bottom). The radial component of current density j_r is shown in colors. Directions of vector field \mathbf{j} are marked by black sticks (not scaled to amplitude for better clarity).

Fig. 3 shows the density of induced electric currents,

$$\mathbf{j} = \frac{1}{\mu_0} \text{curl} \mathbf{B}, \quad (2)$$

in the Earth for some of the conductivity models. The two plots on the top display the longitudinal (westward) component j_φ , at the equator, and at longitude $\varphi = 90^\circ$ as a function of time and radius for 1-D models A and B, respectively. In the case of spherically symmetric models, the electric currents are purely toroidal, the radial component j_r is zero, and j_φ dominates over the colatitudinal (southward) component j_θ which is independent on the dipolar source field, but relies on excitation by the smaller, axially non-symmetric terms. Regardless of the D'' structure, a maximum of j_φ occurs at the depths of 900–1200 km, where an increase of conductivity with depth by almost one order of magnitude was assumed in the 1-D background model. Presence of highly conductive PPV in the D'' in model B is reflected by electrical currents whose amplitude is about 4 times smaller than in the upper mantle, and which are delayed by 20–30 days after the onset of the storm. Currents of similar amplitude flow also in the upper 100 km of the core, and quickly decay with depth due to its high conductivity.

The bottom plot in Fig. 3 shows the effect of more complicated, 3-D conductivity structure in D'' . An instantaneous snapshot at $t = 1998.5995$ years is plotted in an equatorial section through the meridional band of PPV in model D. The lateral conductivity variation gives rise to radial currents j_r . The currents are channeled into the highly-conductive area in D'' both from the surrounding lower mantle, and from the core. In the models E and F (not visualized here) with more complicated D'' structure, the flow of electric currents generally conforms to the same paradigm, i.e., the currents are concentrated in the D'' in the PPV-rich areas, and less conductive PV-dominant barriers are bypassed through the core.

4. 1-D inverse modelling

The 3-D forward modelling described in the previous section provides for each conductivity model $X = \{A, B, C, D, E, F\}$ a com-

plete time series of spherical harmonics representing the internal, induced field, $G_{jm}^{(i,X)}(t)$, up to degree and order 16, and with 1 h sampling rate. These synthetic data are then inverted in terms of 1-D conductivity models, along the lines described in detail by Velínský (2010). Here we present only a short overview. First, Gaussian noise is added to the source dipolar coefficient $G_{10}^{(e)}(t)$, and the synthetic dipolar coefficients $G_{10}^{(i,X)}(t)$,

$$G_{10}^{(e,\varepsilon)}(t) = G_{10}^{(e)}(t) + N\left(0, \frac{4\pi}{3} \varepsilon^2\right)(t), \quad (3)$$

$$G_{10}^{(i,X,\varepsilon)}(t) = G_{10}^{(i,X)}(t) + N\left(0, \frac{4\pi}{3} \varepsilon^2\right)(t). \quad (4)$$

Here $N(0, \cdot)(t)$ denotes the zero-centered normal distribution, and the standard deviation is scaled so that $\varepsilon = 1$ nT corresponds to the 1 nT noise of the horizontal component of magnetic field at the equator on the Earth's surface. The spherical harmonic analysis of 7 years of CHAMP satellite data yields error estimates $\varepsilon \approx 1\text{--}5$ nT, after rescaling to the equator (Velínský, 2010). Here we present results with rather conservative setting of $\varepsilon = 5$ nT.

The model vector $\mathbf{m} = \{\log_{10} \sigma_k\}_{k=1}^K$ is introduced, which consists of logarithms of conductivities in layers, using the same discretization, as in the background 1-D model. Then, the data misfit is defined as

$$\begin{aligned} \chi^2(\mathbf{m}; X; \varepsilon) &= \frac{1}{(t_1 - t_0)} \int_{t_0}^{t_1} \left[\frac{G_{10}^{(i,\varepsilon)}(\mathbf{m}; t) - G_{10}^{(i,X,\varepsilon)}(t)}{\varepsilon} \right]^2 dt \\ &= \frac{1}{N_D} \sum_{i=1}^{N_D} \left[\frac{G_{10}^{(i,\varepsilon)}(\mathbf{m}; t_i) - G_{10}^{(i,X,\varepsilon)}(t_i)}{\varepsilon} \right]^2 \end{aligned} \quad (5)$$

where $G_{10}^{(i,\varepsilon)}(\mathbf{m}; t)$ is the dipolar coefficient of internal field predicted by forward 1-D modelling for a particular conductivity model \mathbf{m} , excited by noisy source $G_{10}^{(e,\varepsilon)}(t)$. Time $t_0 = 720$ h is used to minimize the influence of switch-on effect (Velínský et al., 2006) on the results of inversion. The time integration spans the entire 12 year interval, by setting t_1 to the last hour of year 2008. With time step 1 h, this corresponds to $N_D = 121992$ data points.

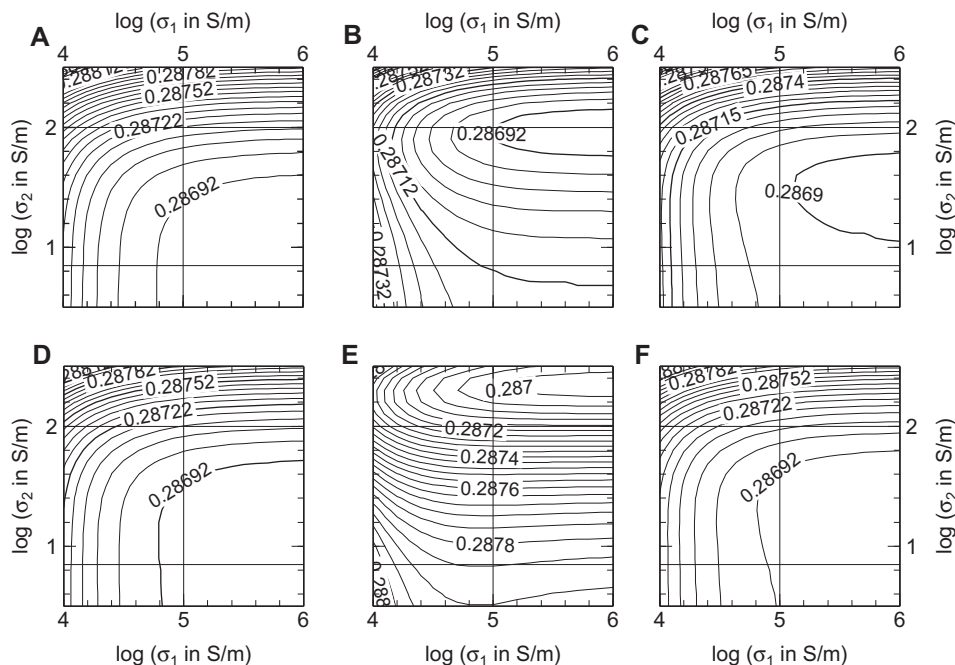


Fig. 4. Misfit χ^2 as function of core conductivity σ_1 , and D' conductivity σ_2 . Isolines of χ^2 are plotted in two-dimensional cross-sections of the parameter space for each respective conductivity model A–F. Assumed conductivities of core, PV and PPV are emphasized by horizontal and vertical grid lines.

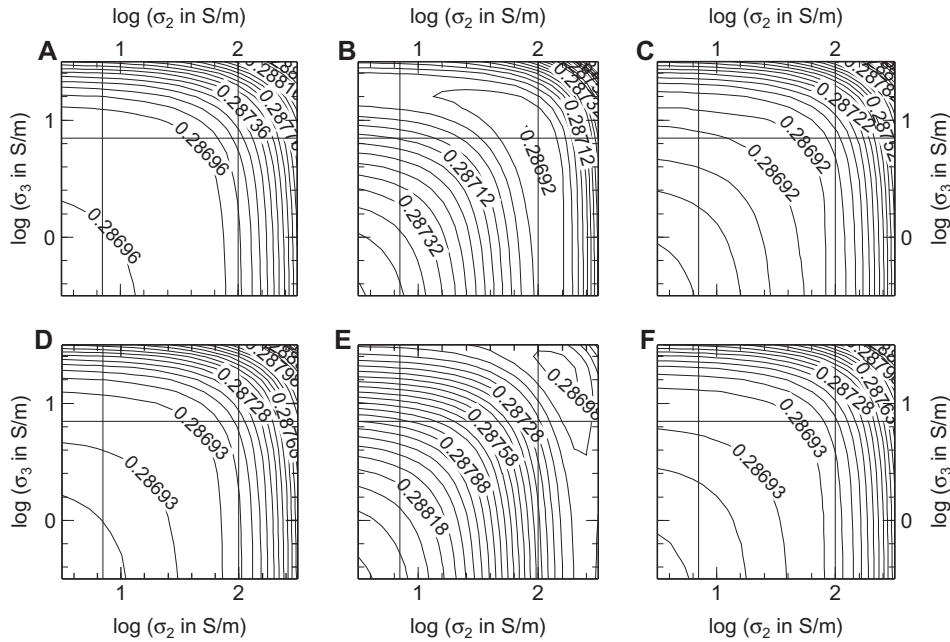


Fig. 5. Misfit χ^2 as function of D'' conductivity σ_2 , and conductivity of the layer just above D'' , σ_3 .

There are three sources of uncertainty in the 1-D inversion of synthetic data. Firstly, the source used in the inversion is spatially inaccurate, using only the dipolar excitation compared to more complicated source in the forward simulation. While this is not an issue in 1-D models A and B, where signals at different spherical harmonics are decoupled, the energy from higher degree and order excitation can leak into dipolar internal field in the case of 3-D models C–F. Secondly, Gaussian noise is added both to the source signal, and induced field. Finally, the true 3-D conductivity model lies outside the space of 1-D conductivity models being explored in cases C–F. Even more realistic approach would consist of evaluation of the induction signals at observatories or along satellite tracks, addition of other magnetic fields (e.g. the main field, and the lithospheric static field, local noise), and reconstruction of both inducing and induced signals from such data. Such a study is outside the scope of this paper.

The problem of χ^2 minimization in the finite-dimensional space of model parameters \mathbf{m} can be tackled by different approaches. Velínský (2010) used the limited memory quasi-Newton technique to find an optimal regularized model. Applying this technique to our synthetic datasets A–F recovers the respective target 1-D conductivity profiles throughout most of the mantle almost perfectly. In order to study the effect of lowermost mantle on the induction response, we revert to a simple technique of parameter search. For each dataset, we match the conductivity with the known target profile, and explore two-dimensional crosssections of the parameter space by varying a pair of parameters: either the core conductivity σ_1 , and the D'' conductivity σ_2 , or σ_2 , and the conductivity σ_3 of a layer just above D'' . Figs. 4 and 5 show the contour lines of χ^2 as function of (σ_1, σ_2) and (σ_2, σ_3) , respectively, for models A–F. All model parameters are varied in steps of 0.1 on the \log_{10} scale.

Starting with the core conductivity σ_1 , Fig. 4 shows that it is correctly recovered in all cases, and it is constrained more strictly from below. Values smaller than the target conductivity of 10^5 S/m imply steeper misfit increase, than values above it. In the 1-D cases A and B, Fig. 5 demonstrates that the conductivities σ_2 , and σ_3 are correctly recovered. Note that the high conductivity of PPV in case B is constrained more sharply by the shape of the misfit function

than in case A where the elongated feature suggests lower sensitivity to σ_2 . 1-D interpretation of datasets C and D demonstrates the effect of interconnection of the conductive PPV with respect to the geometry of the external field. Although both synthetic models contain the same amount of PPV in D'' , the closed electrical loop in the equatorial belt in model C is reflected by a more focused minimum of the misfit recovering higher D'' conductivity. On the other hand, the same amount of PPV arranged in the meridional configuration of model D yields result similar to case A, with smaller and poorly resolved σ_2 . Finally, 1-D inversion of models E and F confirm that the conductivity recovered by 1-D inversions increases both with the PPV content in the lowermost mantle, and its level of interconnection. In case E, the inversion slightly overestimates σ_2 , while the recovered σ_3 matches the average conductivity in the corresponding 3-D layer (using arithmetic averaging of logarithms, i.e., geometric averaging of conductivity). In case F, the average σ_2 and σ_3 are recovered almost perfectly. The overestimation of σ_2 in case E can be explained by the leakage of energy from higher-degree external source field in the 3-D forward modelling. Since it is not accounted for in the 1-D inversion, the additional signal is falsely interpreted by increased conductivity. This effect doesn't appear in cases A and B, where the excitation harmonics are completely decoupled, and can occur to less extent in less conductive cases C, D, and F.

5. Statistical significance of results

The misfit variations shown in Figs. 4 and 5 are obviously very small. The change of conductivity by two orders of magnitude yields less than 10^{-3} relative change of the misfit value χ^2 in some cases. Then the question of significance of such results naturally arises. We will discuss it using the statistical F -test (Chatterjee and Hadi, 2006) in this section. In particular, we test the ability of the data to resolve the model parameters by comparing the misfit obtained by reduced models to the misfit yielded by the full model \mathbf{m} . The F -test assumes normal distribution of data errors, and also requires linearity of the forward problem. The first condition is easily satisfied by our synthetic datasets. As for the second

Table 1

Test of ability to resolve σ_1 and σ_2 using F -test. For each model, and each hypothesis, the table shows the position of the misfit minimum (using the decadic logarithms of conductivities), and the minimum misfit value. The F -test is evaluated in the next column. If it is greater or lower than the critical value F_α , hypothesis H_0 is rejected (R) or accepted (A), respectively, at confidence level α .

Model	H_0		H_1			F	$F_{0.10}$	$F_{0.05}$
	$\sigma_1 = \sigma_2$	χ_0^2	σ_1	σ_2	χ_1^2			
A	3.0	0.292216	6.0	0.6	0.286873	2272.06	R	R
B	3.0	0.291288	6.0	2.0	0.286888	1870.96	R	R
C	3.0	0.291828	6.0	1.5	0.286880	2104.04	R	R
D	3.0	0.292068	6.0	1.1	0.286875	2208.26	R	R
E	3.0	0.290457	6.0	2.4	0.286978	1478.87	R	R
F	3.0	0.291984	6.0	1.4	0.286876	2172.11	R	R

Table 2

Test of ability to resolve σ_2 and σ_3 using F -test.

Model	H_0		H_1			F	$F_{0.10}$	$F_{0.05}$
	$\sigma_2 = \sigma_3$	χ_0^2	σ_2	σ_3	χ_1^2			
A	0.8	0.286899	0.9	0.8	0.286898	0.43	A	A
B	1.2	0.286957	1.9	0.9	0.286918	16.58	R	R
C	1.0	0.286912	1.7	0.6	0.286904	3.40	R	A
D	0.9	0.286901	1.2	0.8	0.286900	0.43	A	A
E	1.5	0.287032	2.2	1.3	0.286960	30.61	R	R
F	0.9	0.286906	1.4	0.8	0.286902	1.70	A	A

condition, while the predicted data $\{G_{10}^{(i,\epsilon)}(\mathbf{m}; t_i)\}_{i=1}^{N_D}$ are nonlinear functions of the logarithms of conductivities assembled in \mathbf{m} , the dependence on the parameters representing the lowermost parts of the model, $\{m_k\}_{k=1}^3$ is weak, and can be linearized.

The first test checks the ability of the synthetic data to resolve the core and the D'' . We formulate the null hypothesis H_0 : “Reduced model, such that $m_1 = m_2$ (i.e., $\sigma_1 = \sigma_2$) is sufficient to adequately explain the data.” H_0 is tested against hypothesis H_1 : “Full model, such that $m_1 \neq m_2$ must be used.” The reduced and full model spaces have respective dimensions $N_0 = K - 1, N_1 = K$. The best fitting reduced and full models yield respective misfits χ_0^2, χ_1^2 . Hypothesis H_0 will be rejected with α probability of false rejection if the value of the F -test,

$$F = \frac{\chi_0^2 - \chi_1^2}{N_1 - N_0} \frac{N_D - N_1}{\chi_1^2} \quad (6)$$

is greater than the critical value of F distribution $F_\alpha(N_1 - N_0, N_D - N_1)$. Table 1 summarizes the results for cases A–F, and confidence levels of $\alpha = 0.05$ and 0.10. The reduced model hypothesis H_0 is safely rejected in all cases. In other words, separation of the core and D'' in the model is necessary to explain adequately the data.

Similar test can be performed to check resolution between D'' and the lower mantle. The null hypothesis H_0 : “Reduced model, such that $m_2 = m_3$ is sufficient” is again tested against the full model. The results are presented in Table 2. The reduced model hypothesis H_0 is rejected in cases B, E, and with 0.10 probability of false rejection also in case C. All these cases have highly conductive PPV present and well interconnected in D'' . When PPV is missing, or poorly interconnected in the equatorial direction, i.e. in cases A, D, and F, the reduced model is sufficient to explain the synthetic data, and the null hypothesis can be accepted.

6. Conclusions

We have performed a series of 3-D forward and 1-D inverse simulations of EM induction in the lowermost Earth’s mantle and

core, excited by transient signals originating in the magnetosphere. We observe that the conductivity of D'' , in particular the spatial distribution of the highly conductive PPV phase, determines the path chosen by the induced electric currents. Smaller values of the lower mantle electrical conductivity imply induced electric currents in the uppermost parts of the core, while the presence of PPV focuses the electric currents in the conductive areas of D'' , electromagnetically shielding the core below.

Interpretation of 1-D inversions of observatory or satellite geomagnetic data with respect to the conductivity of deep parts of the Earth is tricky. The absence of highly conductive D'' in the results of 1-D inversion of CHAMP satellite data (Velínský, 2010) does not necessarily mean that the highly conductive PPV is not present there. Based on our simulations, especially the results of cases D and F, we conclude that a significant amount of PPV can be present in the D'' without being detected by 1-D inversions of EM induction signals. Sufficient condition for this invisibility is that the highly conductive phase is present in isolated patches with poor interconnection in the equatorial direction of prevailing induced currents. On the other hand, existence of a thick homogeneous layer of highly conductive PPV is in contradiction with the 1-D interpretation of CHAMP satellite data. The PPV in the D'' is expected to reflect the distribution of cold masses associated with paleoslab areas in the circum-Pacific belt (Panning and Romanowicz, 2006). It is probably not connected in the equatorial direction due to the presence of hot plume regions below central Pacific and Africa. Therefore, it cannot be detected by means of a 1-D EM induction.

Unfortunately, while inversions of 3-D mantle conductivity structure become computationally feasible, recovery of heterogeneous structures at the bottom of the mantle is hindered by small sensitivity of the method, and lack of sufficiently strong external excitation with different spatial configuration. The EM data inversion is thus not able to put an independent constraint on the PPV distribution.

Acknowledgments

We thank Lars Tøffner-Clausen and Nils Olsen for providing us with the magnetospheric field model, and Zdeněk Martinec for helpful discussion. Comments by two anonymous reviewers are highly appreciated. This research was supported by the Grant Agency of Czech Republic, project No. P210/11/1366.

References

- Ammann, M.W., Brodholt, J.P., Dobson, D.P. 2010. Simulating diffusion. In: Theoretical and Computational Methods in Mineral Physics: Geophysical Applications, Book Series: Reviews in Mineralogy & Geochemistry, vol. 71, pp. 201–224.
- Balasis, G., Egbert, G.D., Maus, S., 2004. Local time effects in satellite estimates of electromagnetic induction transfer functions. *Geophys. Res. Lett.* 31, L16610.
- Carrez, P., Ferre, D., Cordier, P., 2007. Implications for plastic flow in the deep mantle from modelling dislocations in MgSiO_3 minerals. *Nature* 7131, 68–70.
- Chatterjee, S., Hadi, A.S., 2006. Regression Analysis by Example. John Wiley & Sons, Hoboken, ISBN 0471746967, 9780471746966 Length 375 pages.
- Čížková, H., Čadek, O., Matyska, C., Yuen, D.A., 2010. Implications of post-perovskite transport properties for core-mantle dynamics. *Phys. Earth Planet. Int.* 180 (3–4), doi:10.1016/j.pepi.2009.08.008.
- Everett, M.E., Constable, S., Constable, C., 2003. Effects of near-surface conductance on global satellite induction responses. *Geophys. J. Int.* 153, 277–286.
- Fujii, I., Schultz, A., 2002. The 3D electromagnetic response of the Earth to ring current and auroral oval excitation. *Geophys. J. Int.* 151, 689–709.
- Goncharov, A.F., Struzhkin, V.V., Montoya, J.A., Kharlamova, S., Kundargi, R., Siebert, J., Badro, J., Antonangeli, D., Ryerson, F.J., Mao, W., 2010. Effect of composition, structure, and spin state on the thermal conductivity of the Earth’s lower mantle. *Phys. Earth Planet. Int.* 180 (3–4), 148–153.
- Hernlund, J.W., Thomas, C., Tackley, P.J., 2005. A doubling of the post-perovskite phase boundary and structure of the Earth’s lowermost mantle. *Nature* 434 (7035), 882–886.
- Hunt, S.A., Weidner, D.J., Li, L., Wang, L., Walte, N.P., Brodholt, J.P., Dobson, D.P., 2009. Weakening of calcium iridate during its transformation from perovskite to post-perovskite. *Nature Geosci.* 2, 794–797.

- Hutko, A.R., Lay, T., Revenaugh, J., Garnero, E.J., 2008. Anticorrelated seismic velocity anomalies from post-perovskite in the lowermost mantle. *Science* 320 (5879), 1070–1074.
- Kelbert, A., Schultz, A., Egbert, G., 2009. Global electromagnetic induction constraints on transition-zone water content variations. *Nature* 460, 1003–1006.
- Lay, T., Hernlund, J., Garnero, E.J., Thorne, M.S., 2006. A post-Perovskite lens and D' heat flux beneath the central Pacific. *Science* 314, 1272–1276.
- Martinec, Z., Velínský, J., 2009. The adjoint sensitivity method of global electromagnetic induction for CHAMP magnetic data. *Geophys. J. Int.* 179, 1372–1396.
- Matyska, C., Yuen, D.A., 2005. The importance of radiative heat transfer on superplumes in the lower mantle with the new post-perovskite phase change. *Earth Planet. Sci. Lett.* 234 (1–2), 71–81.
- Monnereau, M., Yuen, D.A., 2007. Topology of the postperovskite phase transition and mantle dynamics. *Proc. Natl. Acad. Sci.* 104 (22), 9156–9161.
- Murakami, M., Hirose, K., Kawamura, K., Sata, N., Ohishi, Y., 2004. Post-perovskite phase transition in MgSiO₃. *Science* 7, 855–858.
- Nakagawa, T., Tackley, P.J., 2004. Effects of a perovskite-post perovskite phase change near core-mantle boundary in compressible mantle convection. *Geophys. Res. Lett.* 31 (16), L16611.
- Nakagawa, T., Tackley, P.J., 2005. The interaction between the post-perovskite phase change and a thermo-chemical boundary layer near the core-mantle boundary. *Earth Planet. Sci. Lett.* 238 (1–2), 204–216.
- Nakagawa, T., Tackley, P.J., 2006. Three-dimensional structures and dynamics in the deep mantle: Effects of post-perovskite phase change and deep mantle layering. *Geophys. Res. Lett.* 33 (12), L12S11.
- Oganov, A.R., Ono, S., 2004. Theoretical and experimental evidence for a post-perovskite phase of MgSiO₃ in Earth's D' layer. *Nature* 430, 445–448.
- Oganov, A.R., Ono, S., 2005. The high pressure phase of alumina and implications for Earth's D' layer. *Proc. Natl. Acad. Sci.* 102, 10828–10831.
- Ohta, K., Onoda, S., Hirose, K., Sinmyo, R., Shimizu, K., Sata, N., Ohishi, Y., Yasuhara, A., 2008. The electrical conductivity of post-perovskite in Earth's D' layer. *Science* 320 (5872), 89–91.
- Ohta, K., Hirose, K., Ichiki, M., Shimizu, K., Sata, N., Ohishi, Y., 2010. Electrical conductivities of pyrolytic mantle and MORB materials up to the lowermost mantle conditions. *Earth Planet. Sci. Lett.* 289, 497–502.
- Ono, S., Oganov, A.R., Koyama, T., Shimizu, H., 2006. Stability and compressibility of the high-pressure phases of Al₂O₃ up to 200 GPa: Implications for the electrical conductivity of the base of the lower mantle. *Earth Planet. Sci. Lett.* 246 (3–4), 326–335.
- Panning, M., Romanowicz, B., 2006. A three-dimensional radially anisotropic model of shear velocity in the whole mantle. *Geophys. J. Int.* 167 (1), 361–379.
- Shim, S.H., 2008. The postperovskite transition. *Ann. Rev. Earth Planet. Sci.* 36, 569–599.
- Tackley, P.J., Nakagawa, T., Hernlund, J.W., 2007. Influence of the post-perovskite transition on thermal and thermo-chemical mantle convection, in post-perovskite: The last mantle phase transition. In: *Geophysical Monograph Series*, 174, AGU.
- Tarits, P., Manda, M., 2010. The heterogeneous electrical conductivity structure of the lower mantle. *Phys. Earth Planet. Int.* 183 (1–2), 115–125.
- Tateno, S., Hirose, K., Sata, N., Ohishi, Y., 2009. Determination of post-perovskite phase transition boundary up to 4400 K and implications for thermal structure in D' layer. *Earth Planet. Sci. Lett.* 277 (1–2), 130–136.
- Tosi, N., Yuen, D.A., Čadež, O., 2010. Dynamic consequences in the lower mantle with the post-perovskite phase change and strongly depth-dependent geodynamic and transport properties. *Earth Planet. Sci. Lett.* 298, 229–243.
- Tøffner-Clausen, L., Sabaka, T.J., Olsen, N., 2010. End-to-end mission simulation study (e2e+). In: *Proceedings of the Second International Swarm Science Meeting*, ESA, 2010.
- Tsuchiya, T., Tsuchiya, J., Umemoto, K., Wentzcovitch, R.M., 2004. Phase transition in MgSiO₃ perovskite in the Earth's lower mantle. *Earth Planet. Sci. Lett.* 224, 241–248.
- van den Berg, A.P., de Hoop, M.V., Yuen, D.A., Duchkov, A., van der Hilst, R.D., Jacobs, M.H.G., 2010. Geodynamical modeling and multiscale seismic expression of thermo-chemical heterogeneity and phase transitions in the lowermost mantle. *Phys. Earth Planet. Int.* 180 (3–4), 244–257.
- van der Hilst, R.D., de Hoop, M.V., Wang, S., Shim, L., Tenorio, P., 2007. Seismostratigraphy and thermal structure of Earth's core-mantle boundary region. *Science* 315, 1813–1817.
- Velínský, J., Martinec, Z., 2005. Time-domain, spherical harmonic-finite element approach to transient three-dimensional geomagnetic induction in a spherical heterogeneous Earth. *Geophys. J. Int.* 160, 81–101.
- Velínský, J., Martinec, Z., Everett, M.E., 2006. Electrical conductivity in the Earth's mantle inferred from CHAMP satellite measurements—I. Data processing and 1-D inversion. *Geophys. J. Int.* 166, 529–542.
- Velínský, J., 2010. Electrical conductivity in the lower mantle: Constraints from CHAMP satellite data by time-domain EM induction modeling. *Phys. Earth Planet. Inter.* 180 (3–4). doi:10.1016/j.pepi.2010.02.007.
- Velínský, J., Finlay, C.C., 2011. Effect of a metallic core on transient geomagnetic induction. *Geochem. Geophys. Geosyst.* 12, Q05011.
- Walte, N., Heidelbach, F., Miyajima, N., Frost, D., 2007. Texture development and TEM analysis of deformed CaIrO₃: Implications for the D' layer at the core-mantle boundary. *Geophys. Res. Lett.* 34, L08306.
- Wookey, J., Kendall, J.M., 2008. Constraints on lowermost mantle mineralogy and fabric beneath Siberia from seismic anisotropy. *Earth Planet. Sci. Lett.* 275 (1–2), 32–42.